(U-Th)/He ages of phosphates from Zagami and ALHA77005 Martian meteorites: Implications to shock temperatures

Kyoungwon Min [a],[*], Annette E. Farah [a],[1], Seung Ryeol Lee [b], Jong Ik Lee [c]

[a] *Department of Geological Sciences, University of Florida, Gainesville, FL 32611, USA*
[b] *Korea Institute of Geosciences and Mineral Resources, Daejeon, Republic of Korea*
[c] *Korea Polar Research Institute, Incheon, Republic of Korea*

Abstract

Shock conditions of Martian meteorites provide crucial information about ejection dynamics and original features of the Martian rocks. To better constrain equilibrium shock temperatures ($T_{equi-shock}$) of Martian meteorites, we investigated (U-Th)/He systematics of moderately-shocked (Zagami) and intensively shocked (ALHA77005) Martian meteorites. Multiple phosphate aggregates from Zagami and ALHA77005 yielded overall (U-Th)/He ages 92.2 ± 4.4 Ma (2σ) and 8.4 ± 1.2 Ma, respectively. These ages correspond to fractional losses of 0.49 ± 0.03 (Zagami) and 0.97 ± 0.01 (ALHA77005), assuming that the ejection-related shock event at ~3 Ma is solely responsible for diffusive helium loss since crystallization. For He diffusion modeling, the diffusion domain radius is estimated based on detailed examination of fracture patterns in phosphates using a scanning electron microscope. For Zagami, the diffusion domain radius is estimated to be ~2–9 μm, which is generally consistent with calculations from isothermal heating experiments (1–4 μm). For ALHA77005, the diffusion domain radius of ~4–20 μm is estimated.

Using the newly constrained (U-Th)/He data, diffusion domain radii, and other previously estimated parameters, the conductive cooling models yield $T_{equi-shock}$ estimates of 360–410 °C and 460–560 °C for Zagami and ALHA77005, respectively. According to the sensitivity test, the estimated $T_{equi-shock}$ values are relatively robust to input parameters. The $T_{equi-shock}$ estimates for Zagami are more robust than those for ALHA77005, primarily because Zagami yielded intermediate f_{He} value (0.49) compared to ALHA77005 (0.97). For less intensively shocked Zagami, the He diffusion-based $T_{equi-shock}$ estimates (this study) are significantly higher than expected from previously reported $T_{post-shock}$ values. For intensively shocked ALHA77005, the two independent approaches yielded generally consistent results. Using two other examples of previously studied Martian meteorites (ALHA84001 and Los Angeles), we compared $T_{equi-shock}$ and $T_{post-shock}$ estimates. For intensively shocked meteorites (ALHA77005, Los Angeles), the He diffusion-based approach yield slightly higher or consistent $T_{equi-shock}$ with estimations from $T_{post-shock}$, and the discrepancy between the two methods increases as the intensity of shock increases. The reason for the discrepancy between the two methods, particularly for less-intensively shocked meteorites (Zagami, ALHA84001), remains to be resolved, but we prefer the He diffusion-based approach because its $T_{equi-shock}$ estimates are relatively robust to input parameters.
© 2016 Elsevier Ltd. All rights reserved.

Keywords: Zagami; ALHA77005; Martian meteorite; (U-Th)/He; Shock temperature

[*] Corresponding author.
    E-mail address: kmin@ufl.edu (K. Min).
[1] Address: Department of Materials Science and Engineering, University of Tennessee, Knoxville, TN 37996, USA.

1. INTRODUCTION

Shock impact is one of the most prominent dynamic events to have occurred after the formation of any planetary body in our solar system (Wetherill, 1975; Melosh, 1984). Such near-surface episodes cause an instantaneous temperature increase in the ejected materials, followed by rapid cooling. Constraining shock *P-T* conditions and post-shock cooling paths of meteorites is crucial in at least the following three aspects: (1) understanding ejection processes, (2) evaluating pre-shock features in the meteorites, and (3) testing possible transfer of viable life among different planets. Tremendous effort has been devoted to studying the physical conditions of the shock events (Ahrens and Gregson, 1964; Ahrens et al., 1969; Stöffler, 1971; Melosh, 1989; Stöffler et al., 1986, 1991; Stöffler and Langenhorst, 1994). The most solidly established method to constrain shock *P-T* involves comparing microscopic textures of meteorites with those of artificially shocked terrestrial rocks (summarized in Stöffler et al., 1988). Using the equation of state, shock pressures can be converted to corresponding "post-shock temperatures ($T_{post-shock}$)," which represent temperature increases (ΔT) during the shock relative to the pre-shock temperatures. The shock conditions determined for Martian meteorites are summarized in Nyquist et al. (2001) and re-evaluated by Artemieva and Ivanov (2004) and Fritz et al. (2005).

An alternative way to estimate the shock *T* conditions is using radioisotopic systems that are sensitive to temperature. This approach can provide absolute temperature conditions of the shock event instead of *T* increases (ΔT) that can be constrained through the texture-based approach. $^{40}Ar/^{39}Ar$ method has been used for Martian meteorites because of the rapid diffusion of Ar in maskelynite (or feldspar), the major K-bearing mineral phase in the meteorites. The $^{40}Ar/^{39}Ar$ ages of all Martian meteorites are much older than their times of ejection, because ejection-related shock (1) caused a limited effect on the diffusive loss of Ar (Bogard et al., 1979; Ash et al., 1996; Turner et al., 1997; Bogard and Garrison, 1999; Shuster and Weiss, 2005; Walton et al., 2007; Bogard and Park, 2008), and (2) implanted atmospheric Ar into the target materials (Bogard and Johnson, 1983; Bogard et al., 1984, 1986; Becker and Pepin, 1984; Park et al., 2014). The resulting $^{40}Ar/^{39}Ar$ age spectra can be forward-modeled to provide a set of thermal histories, including the shock *T* conditions of ejection (Weiss et al., 2002), as well as pre-ejection thermal histories (Shuster and Weiss, 2005; Cassata et al., 2010). The (U-Th)/He thermochronometer is more sensitive to temperature than $^{40}Ar/^{39}Ar$, allowing for characterization of short-term, high-*T* events, such as shock impacts on the surface of planetary bodies (e.g., Mars: Schwenzer et al., 2007, 2008), or wildfires that have occurred on the Earth's surface (Mitchell and Reiners, 2003; Reiners et al., 2007). In addition to the high sensitivity to temperature, the (U-Th)/He method has other merits in constraining shock *T* conditions of Martian meteorites: (1) U- and Th-rich minerals (e.g., phosphates) are common in many Martian and other meteorites; (2) the applicable age range of the method spans from the beginning of the solar system

(4.5 Ga; Min et al., 2003) to relatively modern human history (AD 79; Aciego et al., 2003); and (3) He concentration in the Martian atmosphere is negligible (Owen et al., 1977), therefore it is unnecessary to consider atmospheric He contamination for (U-Th)/He age determinations, in contrast to Ar implantation during impact (Bogard and Johnson, 1983; Bogard et al., 1984, 1986; Becker and Pepin, 1984).

Although the high diffusivity of He can provide a means to describe the transient episode, it poses a significant problem for (U-Th)/He thermochronology because the resulting ages from various meteorites are frequently scattered and differ from the expected formation ages (Strutt, 1908, 1909, 1910). Before the late 1980s, when detailed He diffusion properties became known, it was difficult to quantitatively evaluate the meanings of (U-Th)/He ages. Another problem related to (U-Th)/He dating of meteorites is contamination by other sources of ^4He, particularly cosmogenic ^4He (Bauer, 1947). In the early history of (U-Th)/He application to meteorites, the cosmogenic ^4He correction was not properly included in age calculations, resulting in old ages (Paneth et al., 1930; Arrol et al., 1942). Because these two contrasting problems (one tending to yield younger, and the other older ages) were combined, the resulting ages were commonly scattered and considered "unreliable" (summarized in Min, 2005). With these problems in mind, multiple studies were performed for a range of meteorites: iron meteorites (Paneth et al., 1930, 1952), ordinary chondrites (Heymann, 1967; Wasson and Wang, 1991; Alexeev, 1998), and Martian meteorites (Swindle et al., 1995; Schwenzer et al., 2004, 2007, 2008). Most of the ages from these studies were interpreted to measure the time of breakup or collision of parent bodies rather than the time of crystallization. As the He diffusion properties in terrestrial minerals (Reiners and Farley, 1999; Farley, 2000; Reiners et al., 2002) and extraterrestrial phosphates (Min et al., 2003, 2013) became available, and the cosmogenic ^4He abundance was better constrained for a diverse range of meteorite compositions (Heymann, 1967; Eugster, 1988; Alexeev, 1998; reviews in Wieler, 2002; Leya and Masarik, 2009), modern (U-Th)/He dating yielded much more reliable ages for meteoritic samples (Schwenzer et al., 2004, 2007, 2008).

The classical approach to determining (U-Th)/He ages is to use whole rock samples. Helium and U-Th concentrations are measured in different rock chips from the same meteorite (or same type of meteorite), and ages are calculated based on the assumption that U, Th, and He are evenly distributed in the samples. In some instances, the U-Th and He concentrations are measured specifically to obtain (U-Th)/He ages; in others, the ages are simply calculated from the available U-Th and He data in the literature. Because whole rock data are summarized for He (e.g., Schultz and Franke, 2004 contains more than 2000 meteorites, including 20 Martian ones) and for U-Th (e.g., Lodders, 1998 for Martian meteorites), it is relatively easy to calculate whole rock (U-Th)/He "ages".

For Martian meteorites, Schwenzer et al. (2004, 2007, 2008) performed dedicated U-Th-He measurements and estimated what fraction of the total radiogenic ^4He expected from crystallization ages was degassed

(He fractional loss $= f_{He}$) during the last thermal event. In these studies, the fractional loss of He correlated with the pressure conditions of shock metamorphism, which most likely related to the ejection of the body from Mars. This supports the idea that He diffusion is mainly controlled by impact, while other pre-ejection effects (weathering, igneous heating) or post-ejection effects (solar heating, cosmic ray exposure, space weathering, and frictional heating in the Earth's atmosphere) are less significant. The robust preservation of radiogenic ^{4}He in meteorites during delivery to Earth, in contrast to traditional concerns, was also consistent with the old ages found in the Acapulco (Min et al., 2003) and ALH84001 Martian meteorite (Min and Reiners, 2007). According to the calculations based on the He and Ar data in ALH84001, the fractional loss of radiogenic ^{4}He during an extended ($\sim$15 Myr) journey from Mars to Earth should be less than 0.1% (Min and Reiners, 2007). Most Martian meteorites, except chassignites, nakhlites (10–11 Myr), and Dhofar 019 ($\sim$20 Myr: Nyquist et al., 2001), have encountered space exposure of less than $\sim$5 Myr. If the observed correlation between shock pressure and (U-Th)/He age truly indicates that He loss was mainly driven by ejection-related shock, it opens the possibility of improving our understanding of the absolute temperature conditions of shock metamorphism. This approach can be applicable to Martian meteorites that show evidence of single shock, with assumptions that the shock (1) occurred during the ejection from Mars, and (2) is the only process that caused He loss.

One of the significant improvements of (U-Th)/He dating in the past decade is its application to single or multiple phosphate grains in meteorites. Because phosphates are the major U-Th reservoirs in many meteorites, the contribution of radiogenic ^{4}He to the total measured ^{4}He in phosphate is much larger in meteorites than for whole rocks, thus yielding more precise and consistent ages (Min, 2005). The first successful application of modern (U-Th)/He techniques at the single grain scale was for the Acapulco meteorite (Min et al., 2003). Because they had not experienced any major shock metamorphism since crystallization at $\sim$4.55 Ga, the Acapulco apatites were expected to contain large amounts of radiogenic ^{4}He, providing favorable conditions for single grain (U-Th)/He dating. Another merit of this meteorite was its thermal history, which could be readily understood from a wide range of isotopic systems, including ^{147}Sm/^{143}Nd, ^{207}Pb/^{206}Pb, ^{40}Ar/^{39}Ar, as well as Pu fission tracks. The apatite (U-Th)/He ages revealed tight clustering near 4.55 Ga, suggesting rapid cooling of Acapulco down to $\sim$120 °C. Also, He diffusion experiments were performed for two apatite grains, yielding a reasonably good linear trend in the Arrhenius plot. Having shown that single grain (U-Th)/He dating has great potential for unraveling the thermal evolution of meteorites, this method was applied to Martian meteorites (Min et al., 2004; Min and Reiners, 2007) and an ordinary chondrite (Min et al., 2013).

The $T_{post\text{-}shock}$ values are commonly estimated relative to the ambient temperatures ($T_{ambient}$) at the time of impact. The current ambient temperatures of the Martian surface are, however, widely variable: as low as -130 °C near the polar areas during winter nights, and as high as $+20$ °C near equatorial regions on summer days. Therefore, the uncertainty in converting post-shock temperatures to absolute temperatures is at least $\sim$150 °C. Furthermore, calibration errors occur in laboratory shock-recovery experiments. Such errors, which are reported with post-shock temperature estimates, are commonly in the range of 10–150 °C for Martian meteorites (Fritz et al., 2005). When both types of errors are combined, the *absolute* shock temperatures for most Martian meteorites can only be constrained within uncertainties of $\pm$200 °C or greater. Another issue is that the $T_{post\text{-}shock}$ estimates are based on conversion of shock pressures assuming the meteorites follow an equation of state (EOS) established from terrestrial rock samples. However, such a conversion may cause a large uncertainty, as it can be significantly affected by multiple parameters, including mineral assemblage, porosity, fractures, and phase transitions during the shock (Artemieva and Ivanov, 2004).

The primary goals of this research are (1) improving fundamental aspects of the (U-Th)/He thermochronometer in application to phosphates in shocked meteorites, (2) constraining absolute equilibrium shock temperatures for Zagami and ALHA77005 Martian meteorites, and (3) comparing these results with estimates from an independent approach using plagioclase refractive indices and other textures. For these purposes, we performed U-Th-Sm-^{4}He measurements for 17 sample packets (12 Zagami + 5 ALHA77005) composed of $\sim$250 phosphate aggregates (165 Zagami + 83 ALHA77005), examined microscopic textures of 56 phosphates in three (2 Zagami + 1 ALHA77005) thin sections, and modeled the resulting data to estimate the equilibrium shock T conditions.

2. ANALYTICAL PROCEDURES

Small rock chips of Zagami ($\sim$15 mm × 10 mm × 2 mm) and ALHA77005 ($\sim$9 mm × 7 mm × 2 mm, 0.27 g) were carefully crushed and sieved, and the extracted fragments were examined using a scanning electron microscope (SEM: Zeiss EVO MA10). According to the previous study (Shan et al., 2013), the SEM analytical conditions used for this scanning procedure do not cause detectable He loss from apatite samples. Because most of the meteoritic phosphates are irregularly shaped, it is almost impossible to extract phosphate grains without modifying the original grain morphologies. Therefore, we used "phosphate aggregates" (phosphate grains with other phases attached) for (U-Th)/He dating. After phosphate aggregates were identified through automated chemical mapping using SEM, the individual aggregates were further investigated at higher resolutions to examine the morphological relationships between the phosphate and attached phases and to determine semi-quantitative chemical compositions of the phosphates using EDS (Energy Dispersive Spectroscopy).

This analytical procedure was routinely performed for 165 phosphate aggregates selected from Zagami and 83 from ALHA77005. Because our initial attempt to analyze single aggregates yielded negligible ^{4}He signals, we decided to analyze multiple aggregates for precise age determinations. After petrographic examinations, one to twenty

phosphate aggregates of similar linear dimensions were grouped together and wrapped in metal (Pt or Nb) tubes for (U-Th)/He dating. For Zagami, samples were divided into two groups based on dimensions: Group 1 (most aggregates with the linear dimensions of 75–150 μm) and Group 2 (all aggregates of 150–250 μm). For ALHA77005, the two packets (A01-20, A21-40) contained aggregates smaller than those in the remaining three packets (A41-56, AHp123, AHp45). The linear dimensions of individual aggregates and the number of aggregates in each packet are listed in the Appendix (Tables A1–A4).

Twelve batches of Zagami and five of ALHA77005 were arranged. Three Zagami batches (ZAG01, ZAG234, ZAG05: Table A2) and two ALHA77005 (AHp123, AHp45: Table A4) were wrapped in Pt tubes, and the remaining 12 batches were packed in Nb tubes. The sample packets were loaded in a stainless steel planchette, and individual packets were degassed using a diode laser under high vacuum conditions. We performed multiple re-extraction steps per packet to confirm extraction of more than 99% of the total gas in each sample. The extracted gas was mixed with ^{3}He spike, purified with a NP-10 getter, and its (mass 4)/(mass 3) ratios were measured using a quadrupole mass spectrometer. After ^{4}He measurements, the phosphates in 17 packets were dissolved in nitric acid, spiked, and heated at 120 °C for >12 h. The U-Th-Sm abundances of each solution were determined using Element2 ICP-MS. The quality of the entire analytical procedures is monitored using Durango apatite standards that are analyzed in addition to the samples.

Calculating (U-Th)/He ages requires estimating the contribution of cosmogenic ^{4}He to the measured total ^{4}He for each phosphate sample packet. For this calculation, we used the following equation: ^{4}He$_{cos}$ = ^{4}He$_{cos}$ production rate [cm^3/g-Ma] × weight of sample [g] × cosmic ray exposure age [Ma]. The production rate of cosmoegenic isotope is highly dependent on the composition of the target material. For our phosphate aggregate samples, we used the method of Leya and Masarik (2009) using the composition of stoichiometric merrillite (Ca$_9$NaMg(PO$_4$)$_7$), and whole rock compositions of Zagami and ALHA77005 (Lodders, 1998). Because the phosphate aggregates are composed of phosphate and attached phases, we used the average production rate for the merrillite and whole rock. The weight of each sample was calculated from its estimated size and density. The exposure ages of 2.7 Ma and 3.2 Ma were used for Zagami and ALHA77005, respectively (Eugster et al., 1997; Schwenzer et al., 2008). For ALHA77005, the cosmogenic ^{4}He contribution is more significant in the range of 17–71% (Table 1) because the amount of radiogenic ^{4}He is low compared to Zagami. This indicates that the cosmogenic ^{4}He corrections for ALH77005 cause significant errors for the final (U-Th)/He age calculation. For Zagami, however, the contribution of cosmogenic ^{4}He to the total ^{4}He is generally in the range of 1–7%. For error propagation, we assumed the 1 sigma uncertainty of the calculated ^{4}He$_{cos}$ to be 10%.

As explained above, we added a known amount of ^{3}He ("^{3}He spike") to the gas extracted from a sample, and then the mixture was used for (mass 4)/(mass 3) measurements.

For most terrestrial samples, the natural abundance of ^{3}He is very small compared to the ^{3}He spike, and it is therefore commonly neglected for (U-Th)/He age calculation. Meteorites, however, may have significant amounts of cosmogenic ^{3}He (and ^{4}He) because the samples have been exposed to intense cosmic rays in space. For each of the Zagami and ALHA77005 samples, we calculated the abundance of cosmogenic ^{3}He following the similar approach for the ^{4}He$_{cos}$ calculation. All the samples yielded negligible amounts of the cosmogenic ^{3}He with ^{3}He$_{cos}$/(^{3}He$_{cos}$ + ^{3}He$_{spike}$) less than 0.03%.

All the reported ages are alpha-recoil uncorrected ages, and the potential effects of alpha recoil correction are discussed in the following section. The uncertainties of the (U-Th)/He ages are estimated based on Monte-Carlo simulations using the analytical errors of U, Th Sm, and ^{4}He measurements. All the uncertainties are at 2σ level.

To investigate textural characteristics and natural distributions of phosphates, we examined thin sections of Zagami (4709–1 from American Museum of Natural History, USNM6545-4 from Smithsonian National Museum of Natural History) and ALHA77005 (120 from NASA) using an optical microscope and SEM. Particularly, internal fracture patterns in individual phosphate grains were carefully examined because these patterns provide important clues in constraining the diffusion domains.

3. RESULTS

Among the twelve Zagami batches, seven with smaller aggregate dimensions (Group 1) yielded widely scattered (U-Th)/He ages in the range of 19.6 Ma to 132.4 Ma, with a weighted mean of 27.1 Ma. The five batches with larger aggregates (Group 2) resulted in relatively concentrated and older ages ranging from 72.6 Ma to 133.0 Ma with a weighted mean of 86.4 Ma. An overall age was calculated by combining the measured U, Th, Sm, and ^{4}He abundances (Min et al., 2013) for the Group 2 samples. The calculated overall age of 92.2 ± 4.4 Ma (2σ) is indistinguishable from the weighted mean of Group 2. Because the overall age is less sensitive to young and precise individual ages, we consider it to be more representative than the weighted mean. The overall age corresponds to a fractional loss of 0.487 ± 0.025, assuming that the ejection-related shock event at ~3 Ma is solely responsible for diffusive helium loss after the (U-Th)/He clock started at ~177 Ma, the timing of crystallization (Nyquist et al., 2001; Zhou et al., 2013; Yin et al., 2014), or intensive shock event (Bouvier et al., 2008, 2009, 2014) (Fig. 1). The calculated fractional loss is well within the Schultz and Franke's (2004) estimate (0.56 ± 0.18) from whole rock samples and corresponds to the upper limit of the Schwenzer et al.'s (2008) estimate (0.36 ± 0.06).

According to our SEM examinations on Zagami samples, the 2-D areal fraction of phosphate is generally larger than ~70% for Group 1 phosphate aggregates, and widely variable (<10% to ~80%) for Group 2 samples. The phosphate portions exposed at the surface of the aggregates in the Group 2 (larger aggregates) show a similar size to those in Group 1 (smaller aggregates), but the attached phases in

Table 1
(U-Th)/He data of the Zagami and ALHA77005 phosphate aggregate samples.

Sample	Sieve size[*] [µm]	No. Grains[**]	U [fmol]	Th [fmol]	Sm [fmol]	$^4He_{measured}$ [fmol]	$^4He_{cosmogenic}$ [%]	(U-Th)/He Age [Ma]	2σ[***] [Ma]	f_{He}[****]
Zagami										
Group 1										
Z01-20	75–125	20	142.1	874	5457	29.8	1.1%	65.8	7.9	0.64
Z21-40	75–125	20	91.9	680	5554	43.7	0.8%	132.4	19.1	0.26
Z41-60	75–125 (7), 125–150 (13)	20	403.0	1285	7255	18.5	3.5%	19.7	1.6	0.90
Z61-80	125–150 (16), 150–250 (4)	20	293.7	1351	9288	20.4	5.6%	24.4	2.1	0.88
ZAG01	125–150	5	0.0	166	93	4.51	4.8%	86.7	11.5	0.52
ZAG234	125–150	15	149.9	908	1882	9.77	6.7%	19.6	2.3	0.89
ZAG05	125–150	11	3.2	345	1316	8.49	5.7%	74.1	29.0	0.59
Group 2										
Z81-92	150–250	12	249.5	1310	9405	72.7	2.2%	98.5	8.9	0.45
Z93-102	150–250	10	115.6	633	4355	47.0	2.9%	133.0	19.0	0.25
Z103-113	150–250	11	223.0	1363	10542	52.6	2.8%	72.6	6.8	0.59
Z114-123	150–250	10	164.8	766	6123	43.4	3.1%	94.1	11.1	0.48
Z124-134	150–250	11	223.3	1017	7519	51.1	2.9%	83.0	9.0	0.54
Overall Age								92.2	4.4	0.49
ALHA77005										
A01-20	63–150	20	12.1	103	1881	2.79	17%	48.2	46.6	0.74
A21-40	63–150	20	7.73	107	1804	0.71	65%	5.7	6.1	0.98
A41-56	63–150 (8), >180 (8)	16	80.4	261	3249	1.28	71%	2.0	1.2	1.00
AHp123	63–150 (5), 150–180 (10)	15	48.9	728	1135	2.82	32%	6.9	1.4	0.98
AHp45	150–180	12	16.1	560	2044	4.35	24%	17.5	4.3	0.92
Overall Age								8.4	1.2	0.97

[*] Number in parenthesis represents the number of grains corresponding to each size fraction.

[**] Total number of grains analyzed together.

[***] Analytical error only.

[****] Calculated based on the crystallization ages of 179 Ma and 177 Ma for ALHA77005 and Zagami, respectively (Nyquist et al., 2002).
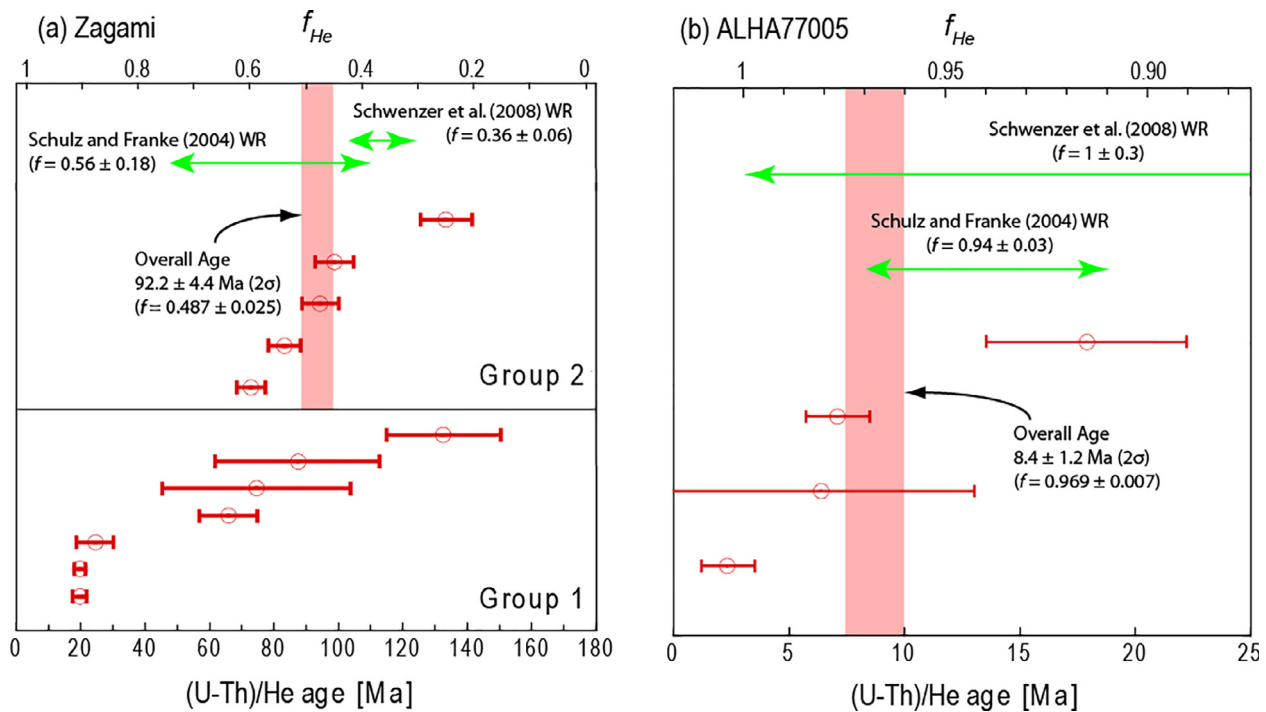
Fig. 1. (U-Th)/He ages from (a) 12 batches of phosphate aggregates from Zagami and (b) 5 batches from ALHA77005. For Zagami, Group 2 phosphate aggregates contain thicker layers of attached phases compared to Group 1 samples. Therefore, the Group 2 phosphate aggregates have retained alpha particles more efficiently, yielding more reliable (U-Th)/He ages. The overall ages are calculated by combining the U, Th, Sm, and ^{4}He abundances measured in each batch. The f_{He} (fractional loss) is estimated based on an assumption that the ejection-related shock event in ~3 Ma is solely responsible for helium loss after a complete reset of the (U-Th)/He clock at 177 Ma and 179 Ma for Zagami and ALHA77005, respectively (Nyquist et al., 2001).

the Group 2 aggregates are generally larger (thickness >~30 μm) than in the Group 1 samples (<~20 μm), resulting in larger overall aggregate sizes. These observations imply that the large aggregates, with thick exotic layers, experienced less alpha-recoil loss; the smaller aggregates' external layers lacked sufficient thickness to shield recoiled alphas, and subsequently yielded apparently younger (U-Th)/He ages. Therefore, we suggest that the ages from Group 2 (larger aggregates) are more reliable than those of Group 1 (smaller aggregates) for Zagami.

The resulting (U-Th)/He ages from Group 1 (smaller aggregates) are more scattered than those from Group 2 (larger aggregates). As stated above, this can be explained by the smaller aggregates experiencing differential degree of alpha recoil loss, depending on the thickness of the attached phases, whereas the larger samples retained most of the alphas. In addition, the shock event is a very heterogeneous phenomenon with localized heating (Artemieva and Ivanov, 2004; Fritz et al., 2005; Beck et al., 2005), before the thermal equilibrium is reached within a time scale of 0.1–1 s (Fritz and Greshake, 2009). This may have caused differential He loss, therefore scattered (U-Th)/He ages.

The five ALHA77005 batches yielded (U-Th)/He ages ranging from 2.0 Ma to 17.5 Ma, with one meaningless age of 48.2 ± 46.6 Ma. The weighted mean of the five ages is 4.6 Ma. The overall age is estimated as 8.4 ± 1.2 Ma, which corresponds to helium fractional loss of 0.969

± 0.007 with an assumed He accumulation since ~179 Ma (Nyquist et al., 2001). This estimate is consistent with findings of Schwenzer et al. (1 ± 0.3; 2008) and Schultz and Franke (0.94 ± 0.03; 2004).

4. THERMAL MODELING AND DISCUSSION

4.1. Modeling parameters

To explain the new phosphate (U-Th)/He ages obtained from Zagami and ALHA77005, we performed thermal modeling with an assumption that the ejected meteoroids reached equilibrium peak temperatures (Fritz et al., 2005) followed by conductive cooling. This modeling requires multiple parameters, including (1) the He diffusion domain radius (r), (2) pre-atmospheric body radius ($R_{pre-atm}$), (3) depth of a sample from the surface of the parent meteoroid (d), (4) ambient temperature of the meteoroid immediately after ejection (T_s), (5) thermal diffusivity (α), and (6) activation energy (E_a) and pre-exponential term (D_o) for He diffusion in merrillite.

4.1.1. He diffusion domain size in phosphate

Diffusion domain size varies widely for different meteorites and can significantly affect the results of the thermal modeling. For unshocked meteoritic phosphates (Min et al., 2013) or terrestrial apatite samples (Reiners and Farley, 2001), it is suggested that the grain itself represents

the He diffusion domain. In contrast, phosphates and other mineral phases in shocked meteorites are very irregular in shape and contain numerous internal fractures that can serve as pathways of rapid He loss. Therefore diffusion domains are smaller than the grain itself. To estimate the diffusion domain radius of merrillite, we carefully examined numerous phosphate grains in Zagami and ALHA77005.

According to BSE (Back-Scattered Electron) images, all of the analyzed phosphate grains in Zagami and ALHA77005 contain numerous internal fractures (Fig. 2). It is clear that the Zagami phosphates contain more dense populations of internal fractures than ALHA77005. The portions bounded by the visible fractures, also called fracture-free areas (FFAs: Min and Reiners, 2007), represent the maximum dimension of He diffusion domains because rapid He diffusion can occur along the fractures. To define FFAs, all the visible internal fractures were traced under SEM at a maximum resolution of ~5–50 nm.

The surface area of each FFA was measured and converted to a radius (=R_{FFA}) of a circle having the same surface area. Fig. 2 displays the results for 3861 FFAs for Zagami and 1133 for ALHA77005. The FFA radius distributions indicate peak locations at 1–4 μm and 3–10 μm for Zagami and ALHA77005, respectively. However, small FFAs are almost always more abundant than large FFAs, although their contributions to the (U-Th)/He ages are less significant; therefore, the FFA data must be weighted. We used a simple weighting method of multiplying the frequency by $(R_{FFA})^2$, to incorporate the 2-dimensional contribution of each FFA. This weighting procedure assumes that (1) the spatial distribution of fractures on the vertical dimension (perpendicular to the surface of a thin section) is random and unrelated to the fracture distribution on the horizontal dimension (the surface of a thin section), and (2) the R_{FFA} distribution of the vertical dimension is identical to the R_{FFA} distribution estimated for the
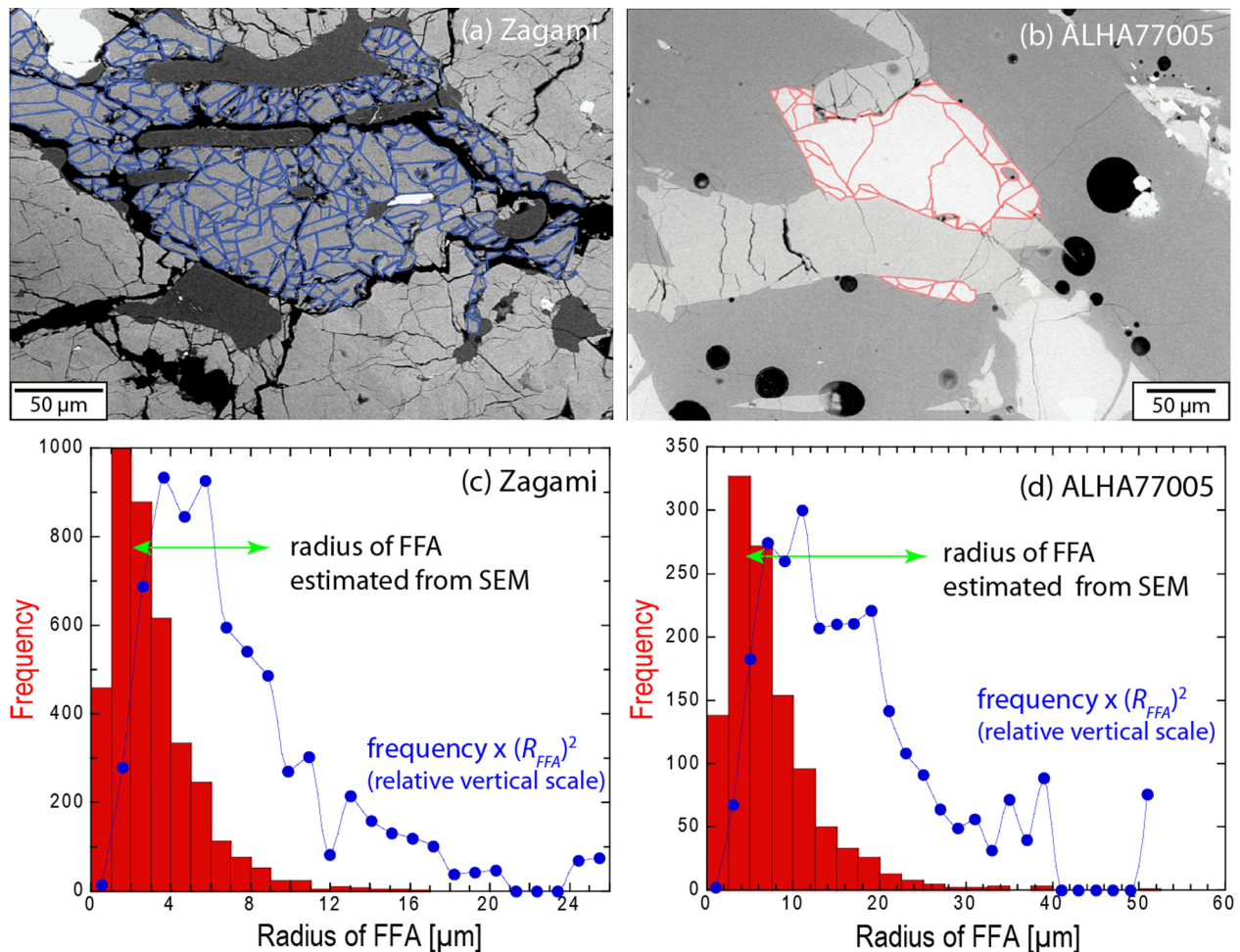

Fig. 2. (a, b) BSE images of phosphates from Zagami and ALHA77005. Traced fracture patterns clearly demonstrate that the Zagami phosphate contains more densely populated fractures than the ALHA 77005 phosphate. (c, d) Radius distributions of fracture-free areas (FFAs) defined from the BSE images. The FFAs represent the maximum dimension of He diffusion domains because rapid He diffusion can occur along the fractures. Small FFAs are almost always more abundant than large FFAs, although their contributions to the (U-Th)/He ages are less significant. Therefore, the FFA data must be weighted. The filled circles represent the weighted FFA distributions to incorporate 2-dimensional contribution of each FFA. The peaks are at ~2–9 μm for Zagami, and 5–20 μm for ALHA77005.

horizontal dimension (Min and Reiners, 2007). This procedure weighs more for the larger FFAs, resulting in the FFA distributions with peaks at ~2–9 μm for Zagami, and 5–20 μm for ALHA77005.

Another way to constrain the diffusion domain size is through stepped heating experiments. For a Zagami whole rock sample, Bogard et al. (1984) reported ~11% He loss during a laboratory heating at 350 °C. Assuming that helium diffusion during the stepped heating experiments follows the Arrhenius relationship determined for Guarena merrillite (Min et al., 2013), we calculated He fractional loss for a range of diffusion domain radii (Fig. 3). For a homogeneous initial He distribution in diffusion domains, the observed 11% He loss during the lab experiments corresponds to a diffusion domain radius of ~3–4 μm depending on the heating durations (Fig. 3). However, it is likely that the natural He distribution in Zagami phosphates before the stepped heating experiments have displayed a gradual decrease of He concentration from the core to the rim because Zagami experienced partial He degassing during the shock event. A diffusion domain, showing such a He concentration gradient, is expected to yield less diffusive He loss than a domain with homogeneous initial He distribution at the same laboratory heating conditions. To assess the initial He gradient effect, we generated a He concentration profile experiencing 50% He loss (comparable to 48% He loss identified from the new (U-Th)/He ages from Zagami; Fig. 1) induced by arbitrarily selected heating conditions at 350 °C for variable durations. Then, the relationship between the resulting fractional loss and diffusion domain radius was calculated for the isothermal heating

described in Bogard et al. (1984). The diffusion domain radius corresponding to the observed 11% He loss is 1–1.5 μm. Although the natural He concentration profiles in the diffusion domains have yet to be clarified, this approach suggests the realistic diffusion domain radius is probably in the range of 1–4 μm.

The diffusion domain radius estimated from the lab heating experiments (1–4 μm) is consistent with or slightly lower than the R_{FFA} determined from the SEM image analysis (2–9 μm). The minor discrepancy is probably derived from microfractures not identified during our SEM analysis. These results suggest that the FFAs determined from SEM image analysis can provide a good first order estimation on the He diffusion domain size even for heavily fractured merrillite samples such as those found in shocked Martian meteorites.

For ALHA77005, we could not obtain any low temperature step heating data; therefore, we were unable to check the reliability of our estimate of diffusion domain radius based on the FFAs. However, the FFAs defined in ALHA77005 are much cleaner and more homogeneous than the Zagami samples in the SEM images, suggesting that the effect of invisible microfractures would be less in ALHA77005.

4.1.2. Radius of the parent meteoroid

The pre-atmospheric body radius ($R_{pre-atm}$) of Zagami was mainly constrained by cosmogenic isotope data. Based on ^{26}Al, ^{10}Be, and ^{53}Mn isotopes, Schnabel et al. (2001) suggested $R_{pre-atm}$ of 25 cm for Zagami. This is confirmed by Eugster et al. (2002), who investigated Kr isotopic com-
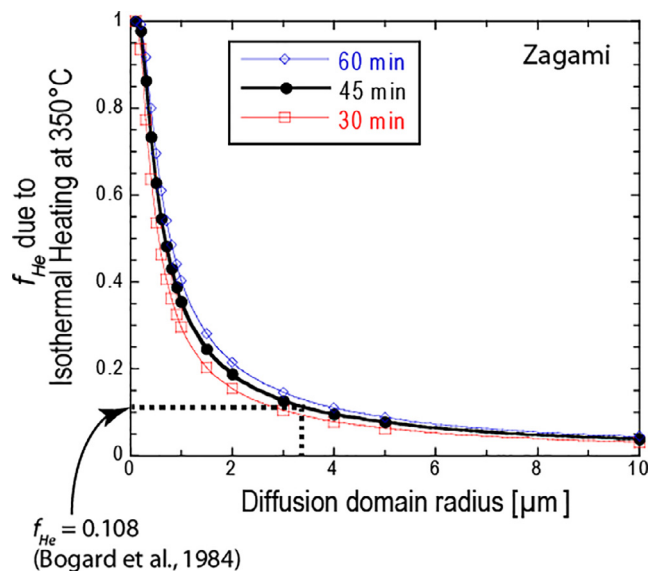

Fig. 3. Relationship between He fractional loss during isothermal heating at 350 °C and diffusion domain radius of phosphate. It is assumed that the He was homogeneously distributed in the sample before the laboratory heating experiments. Helium diffusion properties of Guarena merrillite (Min et al., 2013) are used for the calculation. The reported He loss of ~11% during the isothermal heating (Bogard et al., 1984) corresponds to a diffusion domain radius of ~3–4 μm. For a rounded He concentration profile, which is more likely in Zagami phosphates, the corresponding diffusion domain radius slightly decreases to yield the same fractional loss. Because the natural He concentration profiles in the diffusion domains are not known, we suggest that the diffusion domain radius is probably in the range of 1–4 μm for Zagami. The heating duration of the experiment is not specified in the original paper (Bogard et al., 1984), but the senior author of the paper indicated it was ~45 min (see Bogard and Hirsch, 1980).

positions and concluded that the minimum $R_{pre\text{-}atm}$ values for a series of Martian meteorites are in the range of 22–25 cm (23 ± 1 cm for Zagami). Furthermore, hydrodynamic modeling (Artemieva and Ivanov, 2004) suggests high survivability for fragments larger than $\sim$14–20 cm during their passage in Martian atmosphere, supporting previous $R_{pre\text{-}atm}$ estimates. Fritz et al. (2005) also reached similar conclusions regarding the $R_{pre\text{-}atm}$ (20–30 cm) based on thermal history modeling, which would explain the observed plagioclase recrystallization in Martian meteorites. For ALHA77005, Nishiizumi et al. (1986) suggested a $R_{pre\text{-}atm}$ of 5–6 cm based on cosmogenic isotopes of ^{10}Be and ^{36}Cl with an assumed atmospheric ablation thickness of 1–2 cm. Schnabel et al. (2001) suggested a slightly larger $R_{pre\text{-}atm}$ of 10 cm from ^{26}Al, ^{10}Be, and ^{53}Mn isotopes. However, Fritz et al. (2005) suggested a larger radius of 20–30 cm for ALHA77005 because it shows evidence of significant, but not complete, recrystallization of plagioclase, which requires a prolonged stay at high temperatures. One way to explain the discrepancy derived from the two independent approaches is the large size of the parent meteoroid of ALHA77005 ($R_{pre\text{-}atm} = 20$–30 cm) when ejected from Mars. Soon after ejection, the meteoroid experienced a breakup to smaller pieces ($R_{pre\text{-}atm} = 5$–10 cm), corresponding to the size determined from the cosmogenic isotope signatures. Because our thermal modeling is for the first few hours following ejection from Mars, we used the $R_{pre\text{-}atm}$ estimates of 23 cm and 25 cm for Zagami and ALHA77005 for our modeling (Fritz et al., 2005).

4.1.3. Depth of sample

The depth of a sample from the surface of its parent meteoroid (d) is also required for thermal modeling because the conductive cooling path varies depending on d, therefore yielding differential degrees of He degassing. For Zagami, the rock chip sample used for this study was retrieved approximately 5–8 cm below the fusion crust of the recovered Zagami meteorite. Because the parent body should have experienced physical ablation during its entry into Earth's atmosphere, the original parent body at the time of ejection from Mars is expected to be larger. The total mass of the recovered Zagami is $\sim$18 kg, which can be converted to a radius of $\sim$11 cm assuming a spherical geometry (Schwenzer et al., 2007). Considering the estimated $R_{pre\text{-}atm}$ of $\sim$23 cm (Eugster et al., 2002), the d at the time of ejection is estimated as $\sim$17–20 cm ($=(R_{pre\text{-}atm} - R_{recovered\ Zagami}) +$ distance below fusion crust $= (23$–11$) + (5 \sim 8))$ for Zagami. The ALHA77005 sample used in our study (ALHA77005.220.96) is from the large piece produced during the primary cut performed in 1978. Although the exact sample location is not identified, the estimated $R_{pre\text{-}atm}$ (20–30 cm; Fritz et al., 2005) and the meteorite radius ($\sim$3.4 cm; Schwenzer et al., 2007) suggest that a significant portion of the primary meteoroid was removed during its delivery to Earth's surface. From these data, we calculated the d as 22–24 cm for ALHA77005.

4.1.4. Surface temperature

The surface temperature of meteoroid at Martian orbit is estimated approximately (-50 °C) for light chondrites based on their hemispherical emittances (Butler, 1966). This estimate is assumed to be the surface T of Martian meteoroids (T_s) during the first few hours of their journey in space.

The temperatures between Earth's ($\sim$0 °C) and Mars's ($\sim$$-50$ °C) orbits are low, and the duration of travel is relatively short ($\sim$3 Myr). Zagami and ALHA77005 are therefore not likely to have experienced diffusive He loss during their journeys from Mars to Earth. Even for ALH84001, which experienced a relatively long journey from Mars to Earth ($\sim$15 Myr), similar conclusions were made by comparing Ar and He data (Min and Reiners, 2007).

The T conditions of meteoroid surface during its passage in the Earth's atmosphere are variable. Combining thermoluminescence data from a few meteorites containing fusion crust, Melcher (1979) concluded that the T increase will diminish as a function of distance from the meteoroid surface at a rate of $\sim$51 °C/mm. It was also suggested that the frictional heating in Earth's atmosphere causes a T increase less than 200 °C for the portion that is $\sim$5 mm away from the surface of a meteorite. We performed preliminary He diffusion modeling for a maximum T of 200 °C and heating durations of 10–100 s, the nominal timescale of atmospheric passage of a meteoroid. For a merrillite having a diffusion radius of 5 μm, the resulting diffusive He loss is calculated in the range of $\sim$0.4% ($t = 10$ s) to 1.2% ($t = 100$ s), even at the maximum T of 200 °C. Because the rock chips used for our study were more than 5 mm away from the fusion crust, the T increase is expected to be lower than 200 °C. Therefore, the effect of frictional heating during the passage in Earth's atmosphere is insignificant for our samples.

4.1.5. Thermal diffusivity

Thermal diffusivity (α) is defined as $\frac{k}{\rho C_p}$ where $k =$ thermal conductivity, $\rho =$ density, and $C_p =$ heat capacity. For a shocked shergottite of Los Angeles, Opeil et al. (2010, 2012) measured thermal conductivities at various temperatures. They concluded that the determined thermal conductivities were significantly lower than previous estimates, probably due to many fractures in the shergottite sample. They also observed C_p systematically increasing from 250 J/kg-K (at 100 K) to 750 J/kg-K (at 300 K). These results, combined with the bulk density of typical shergottites ($\sim$2.8–2.9 g/cm^3; McSween, 2002), yield thermal diffusivities (α) of $\sim$7.0 $\times$ 10^{-7} m^2/s at 100 K to $\sim$4.2 $\times$ 10^{-7} m^2/s at 300 K. These new α values are lower than previous estimates (e.g., 17 $\times$ 10^{-7} m^2/s at 300 K) calculated by Fritz et al. (2005) from available C_p (Lu et al., 1994; Waples and Waples, 2004) and k (Hofmeister, 1999) for terrestrial rock samples. A linear extrapolation of the newly measured k and C_p data to higher temperatures results in thermal diffusivity values close to 1 $\times$ 10^{-7} m^2/s ($=$0.001 cm^2/s) for $T > \sim$500 K. We used this updated value for our modeling.

4.1.6. He diffusion properties

The He diffusion properties in meteoritic merrillite and apatite are recently documented from ^{3}He/^{4}He stepped heating experiments on the Guarena chondrite (Min

et al., 2013). The results indicate that the He diffusion in merrillite is significantly slower than in apatite, yielding higher closure temperatures (~110 °C for a grain radius of 25 μm at a cooling rate of ~10 °C/Ma). The updated diffusion parameters for merrillite ($D_o = 0.012$ cm^2/sec, $E = 32.44$ kcal/mol) were used for the thermal modeling.

4.2. Modeling results and sensitivity test

The equilibrium shock temperature ($T_{equi-shock}$: shock T when a meteoroid reached thermal equilibrium) was estimated using the previously explained parameters explained and the following assumptions: (1) the meteoroid experienced conductive cooling after reaching $T_{equi-shock}$ at ~3 Ma, and (2) the ejection-related shock is the single event responsible for He loss following previous complete reset of (U-Th)/He clock at 177 Ma and 179 Ma for Zagami and ALHA77005, respectively. Fig. 4 shows the modeled f_{He} vs $T_{equi-shock}$ at different diffusion domain radii. For Zagami, the $T_{equi-shock}$ is approximately in the range of 360–410 °C (367 °C) at the most likely diffusion domain radius of 2–9 μm (3 μm). For ALHA77005, the $T_{equi-shock}$ is estimated as 460–560 °C (521 °C) at a diffusion domain radius of 5–20 μm (12.5 μm).

To examine how sensitive our $T_{equi-shock}$ estimates are to the input parameters, we performed a sensitivity test. For Zagami, peak temperatures were recalculated for relatively conservative ranges of A (23 ± 4 cm), d (18.5 ± 4 cm), and T_s (-50 ± 40 °C) at a diffusion domain radius (3 μm) and f_{He} (0.49) (Fig. 5). For ALHA77005, we tested for parameters of A (25 +4/−2 cm), d (23 +2/−3 cm) and T_s (−50 ± 40 °C) at a given diffusion domain radius (12.5 cm) and f_{He} (0.97). As shown in Fig. 5, the estimated $T_{equi-shock}$ for Zagami varies within +8/−4 °C for the stated ranges of A and d. Also, the $T_{equi-shock}$ dependence on the surface temperature (T_s) is very small (±1 °C) suggesting that the modeling is robust to the large T fluctuations on Martian surface. For ALHA77005, the estimated $T_{equi-shock}$ varies within +6/−7 °C for A and d. These results suggest that our model $T_{equi-shock}$ calculation is relatively robust to A, d and T_s.

Alpha recoil is another important factor that can yield a biased (U-Th)/He age, f_{He}, and $T_{equi-shock}$ (Fig. 5). For Zagami (Group 2) and ALHA77005, the overall (U-Th)/He ages are identical to the previously reported whole rock ages within their uncertainties, suggesting that the alpha recoil loss from the selected phosphate aggregates is minimal. The similar results were reported for St. Severin chondrite (Min et al., 2013) and ALH84001 Martian meteorite (Min and Reiners, 2007). The most likely explanation for these results is that the phosphate aggregates are composed of phosphate surrounded by other phases; therefore, a
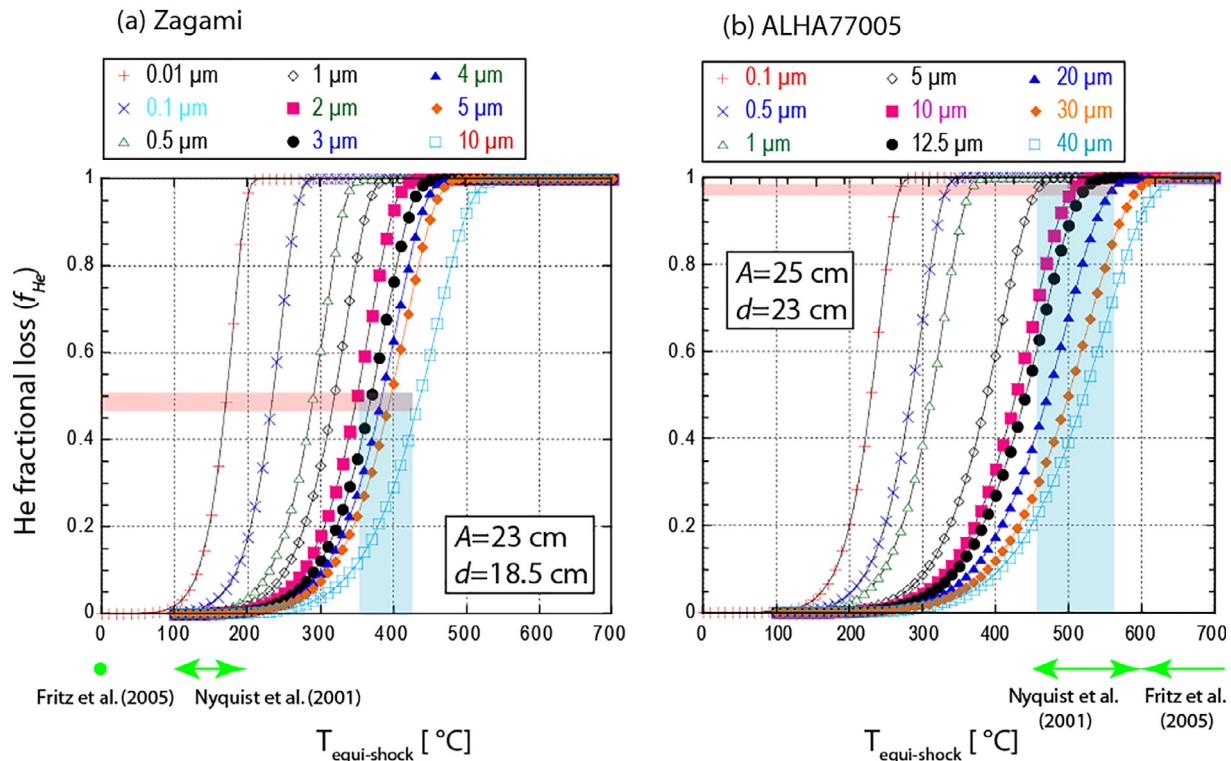

Fig. 4. Thermal modeling results showing a relationship between f_{He} and $T_{equi-shock}$ for (a) Zagami and (b) ALHA77005. It is assumed that the entire parent meteoroid body reached peak temperature instantaneously after a shock, followed by conductive cooling. For the observed f_{He} values (Fig. 1) and the diffusion domain radii (Figs. 2 and 3), the peak temperature conditions can be estimated using this relationship. All the input parameters are discussed in the text. Zagami's f_{He} value (0.49) is intermediate, corresponding to a segment of a steep slope in the $f_{He} - T_{equi-shock}$ plot. Therefore, the $T_{equi-shock}$ estimates are more robust compared to ALHA77005, which yields a rather extreme f_{He} value (0.97).
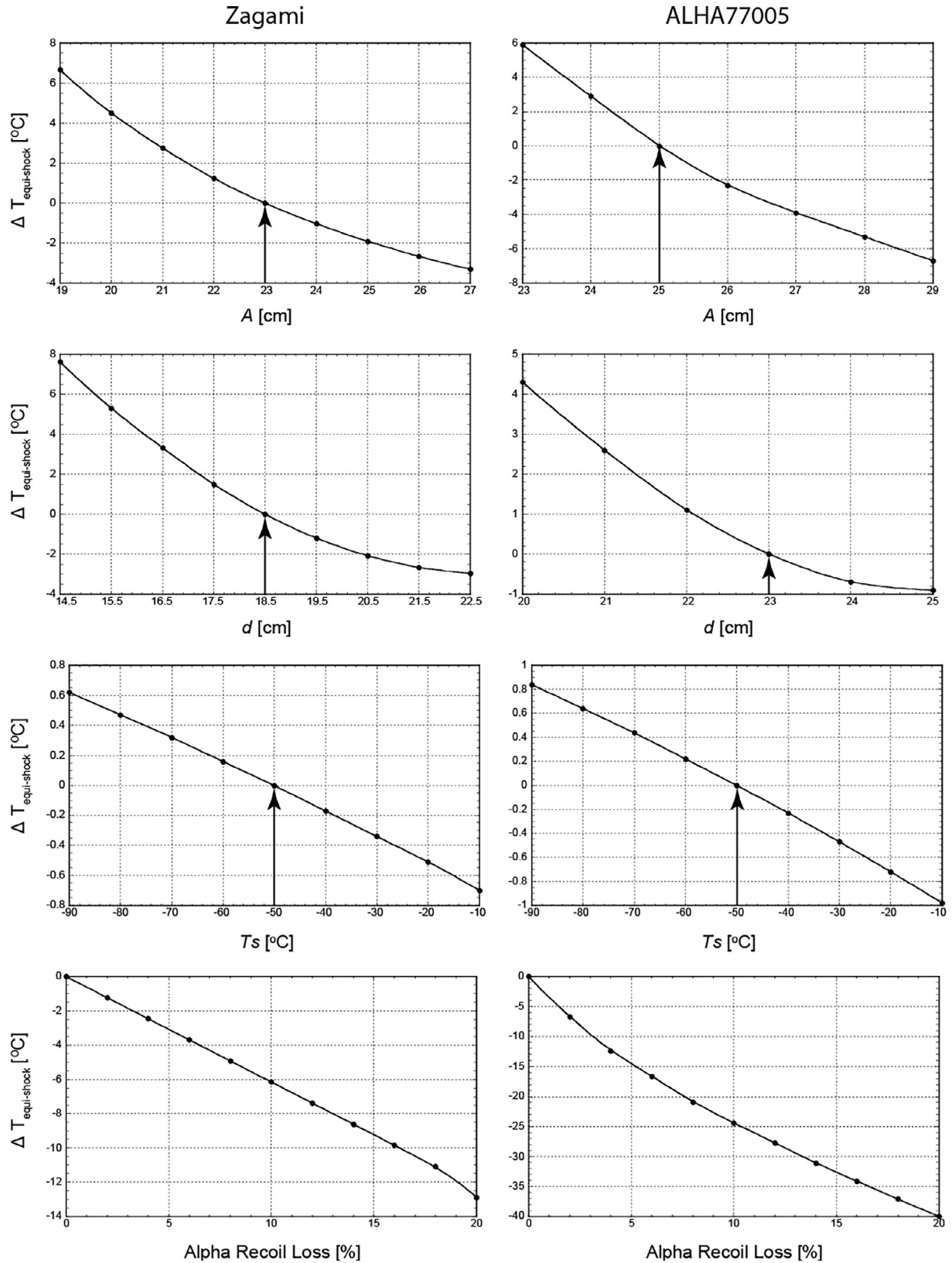
Fig. 5. Sensitivity test results for $T_{equi-shock}$ estimates. The modeled $T_{equi-shock}$ values are relatively robust to variations of A (radius of parent meteoroid), d (depth of sample in parent meteoroid) and T_s (surface temperature of parent meteoroid). Alpha recoil loss can yield also a biased (U-Th)/He age, and thus f_{He} and $T_{equi-shock}$. Although it is likely that the alpha recoil loss is not significant for the samples used for the modeling, alpha recoil loss of 10–20% can lower $T_{equi-shock}$ estimates by 6–13 °C and ~25–40 °C for Zagami and ALHA77005, respectively.

significant amount of alpha particles ejected from phosphates are still preserved within the aggregates. Also, the phosphate grain exposed on the surface of the aggregate likely represents the fracture boundary within an originally large phosphate; in this case, the net alpha loss is zero because the alpha input and output are balanced (Min, 2005). Although we believe the alpha ejection from the aggregates is relatively minor, we tested sensitivity of our $T_{equi\text{-}shock}$ estimates to the alpha recoil loss. As shown in Fig. 5, 20% alpha recoil loss would reduce the $T_{equi\text{-}shock}$ estimate by only ∼13 °C, suggesting that the $T_{equi\text{-}shock}$ estimated for Zagami is robust to the alpha recoil effect. This is also related to the steep slope of the fractional loss curves (Fig. 4), which causes only limited shift of $T_{equi\text{-}shock}$ over a wide change of f_{He} near the Zagami's f_{He} value (0.49). As illustrated in Fig. 4, the $f_{He} - T_{equi\text{-}shock}$ curves display gentle slopes for low (<5%) or high (>95%) fractional loss values. In contrast, the sections corresponding to intermediate f_{He} have steep slopes, indicating that the peak shock temperature estimates are relatively insensitive to f_{He} (or age) for Zagami. This is why the alpha recoil effect, which increases (U-Th)/He ages, has very limited effect on the $T_{equi\text{-}shock}$ estimates. The ALHA77005's f_{He} is 0.97, corresponding to the relatively gentle slope in the $f_{He} - T_{equi\text{-}shock}$ curve (Fig. 4); therefore, the $T_{equi\text{-}shock}$ estimate is more sensitive to input parameters than the estimate for Zagami. Thus, the modeled $T_{equi\text{-}shock}$ of ALHA77005 is lowered by ∼25 °C and ∼40 °C for alpha recoil loss of 10% and 20%, respectively.

One of the assumptions of our thermal modeling is that the ejection-related shock is solely responsible for ^{4}He loss from the samples. This assumption is based on textural and petrographic observations, which suggest no evidence of multiple shock events for these meteorites. Although our assumption is reasonable, we examined how various thermal scenarios can affect our $T_{equi\text{-}shock}$ estimates. If another degassing event were to occur, the ejection-related shock event would be responsible only for partial ^{4}He loss; therefore, the $T_{equi\text{-}shock}$ is expected to be lower than our original estimates. Fig. 6 shows how an additional hypothetical degassing event prior to the ejection can affect the $T_{equi\text{-}shock}$ estimates for Zagami and ALHA77005. If such an additional thermal event occurred in Zagami at 120 Ma and caused 10% fractional loss of radiogenic ^{4}He produced by then, the measured ^{4}He at present could be explained by a $T_{equi\text{-}shock}$ of ∼360 °C at the time of ejection, assuming all the other input parameters remained same. This value is ∼7 °C lower than the $T_{equi\text{-}shock}$ estimate (367 °C) without the hypothetical second thermal event. It is clear that a more recent thermal disturbance would have caused more ^{4}He degassing even for the same fractional loss during the hypothetical event because more ^{4}He atoms would accumulate with the additional time. We tested for instantaneous fractional losses of 10%, 20%, and 30% occurred at any stage after crystallization. At a rather extreme He fractional loss of 30% at a relatively young age of 10 Ma, the $T_{equi\text{-}shock}$ is reduced by 52 °C for Zagami (Fig. 6a). Similarly, the $T_{equi\text{-}shock}$ estimates for ALHA77005 become lower as the fractional loss of additional thermal event increases and the timing of such an event approaches to present. An additional ^{4}He loss of 30% at 10 Ma reduces the $T_{equi\text{-}shock}$ to 466 °C (Fig. 6b); that is 55 °C lower than original estimate of 521 °C calculated. Therefore, the estimated $T_{equi\text{-}shock}$ can be lowered by an additional hypothetical thermal event(s), and the extent of deviation depends on the timing and intensity of the additional event. The modeling also suggests that the
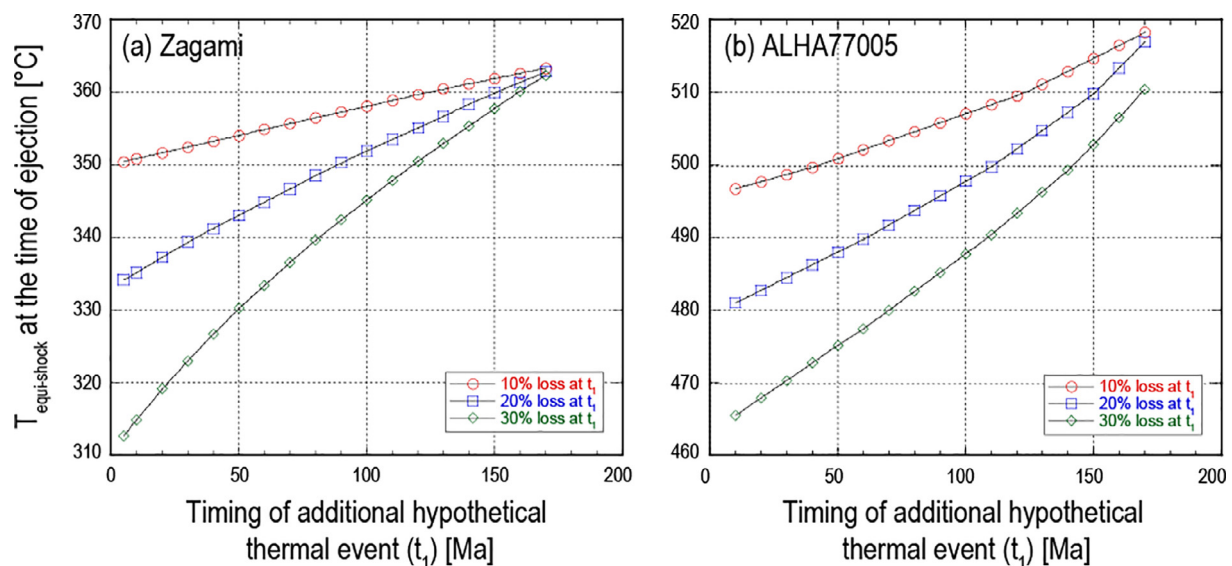

Fig. 6. Relationship between $T_{equi\text{-}shock}$ and t_1 (timing of a hypothetical pre-ejection degassing event). The same parameters used for description of the ejection-related event are employed for this calculation. Three curves represent $T_{equi\text{-}shock}$ variation if instantaneous fractional losses of 10%, 20%, and 30% occur at the given t_1. Such an additional degassing event decreases $T_{equi\text{-}shock}$ because the ejection-related shock is responsible only for a portion of the total ^{4}He loss. A more recent hypothetical degassing event would increase ^{4}He degassing even for the same fractional loss because more ^{4}He atoms would accumulate by that later time. The estimated $T_{equi\text{-}shock}$ decreases more significantly for ALHA77005 than for Zagami at the same t_1 and fractional loss. For the specified fractional losses (10–30%), the extent of $T_{equi\text{-}shock}$ reduction is less than ∼50 °C for both Zagami and ALHA77005.

extent of such deviation is probably less than ~50 °C for both Zagami and ALHA77005.

4.3. Comparison with previous estimates

The shock temperature conditions ($T_{equi\text{-}shock}$) of meteorites can be indirectly constrained using the refractive indices of feldspars and other textural evidence calibrated against artificially shocked rock samples (Stöffler et al., 1988). However, the reliability of these methods has been seriously questioned (El Goresy et al., 2013). These traditional methods can provide post-shock temperatures ($T_{post\text{-}shock}$), which represent "temperature increases" during the shock event relative to the ambient temperature ($T_{ambient}$) at the time of shock. A conversion of the $T_{post\text{-}shock}$ to absolute equilibrium shock temperature ($T_{equi\text{-}shock}$) requires information on $T_{ambient}$ for the following equation: $T_{equi\text{-}shock} = T_{post\text{-}shock} + T_{ambient}$. All Martian meteorites are believed to be derived from relatively shallow locations in the Martian crust (Artemieva and Ivanov, 2004). Therefore, their ambient temperatures at the time of impact are significantly affected by the Martian surface temperatures, which in turn vary widely depending on the latitude, elevation, and time (season, hours). For example, the surface temperatures of five landing sites (Viking 1, Viking 2, Mars Pathfinder, Spirit, Opportunity) at latitudes lower than 50° fluctuate between 160–290 K (Ulrich et al., 2010). The average temperatures at higher latitudes are expected to be even lower by at least a few tens of degrees (Tellmann et al., 2013). Because the locations of the parent bodies and the timing (e.g., day or night, summer or winter) of ejection of the Martian meteorites are highly uncertain, $T_{ambient}$ can be constrained no better than the minimum Martian surface T variation of ~150 °C (or K).

For Zagami, the $T_{post\text{-}shock}$ was estimated as 220 ± 50 °C (Stöffler et al., 1986; Nyquist et al., 2001). However, a significantly lower estimate of 70 ± 5 °C was suggested in a recent study (Fritz et al., 2005). The cause of the inconsistent estimates is unclear. Assuming the ambient Martian surface T ($T_{ambient}$) in the range of 140–290 K, the estimated $T_{post\text{-}shock}$ of 220 ± 50 °C (Stöffler et al., 1986; Nyquist et al., 2001) can be converted to minimum $T_{equi\text{-}shock}$ of 87 ± 50 °C (=220 ± 50 K + 140 K = 360 ± 50 K = 87 ± 50 °C) and maximum $T_{equi\text{-}shock}$ of 237 ± 50 °C (=220 ± 50 K + 290 ± 50 K = 510 ± 50 K = 237 ± 50 °C). For the lower $T_{post\text{-}shock}$ estimate of 70 ± 5 °C (Fritz et al., 2005), the $T_{equi\text{-}shock}$ can be calculated in the same way with the resulting estimates in the range of −63 ± 5 °C and 87 ± 5 °C. Our $T_{equi\text{-}shock}$ estimate (367 °C or slightly lower) is significantly higher than these estimates, even with the large uncertainties related to the conversion.

For ALHA77005, the traditional method also yields two inconsistent $T_{post\text{-}shock}$ estimates: 450–600 °C (Nyquist et al., 2001) and 800 ± 200 °C (Fritz et al., 2005). The large uncertainties associated with the $T_{post\text{-}shock}$ and $T_{ambient}$ hamper precise estimation of $T_{equi\text{-}shock}$. These estimates can be converted to $T_{equi\text{-}shock}$ of 317–617 °C and 467–1017 °C, respectively, considering the T variation of Martian surface. Our $T_{equi\text{-}shock}$ estimate (521 °C or slightly lower) is consistent

with these two previous estimates, but with a significantly higher precision.

Because temperature at the surface of meteoroid is one of the parameters for thermal modeling, perhaps Martian surface T variations can also affect He diffusion modeling. However, diffusive loss of He is a continuous process in the hours following shock impact. Assuming a meteoroid were to fly faster than the escape velocity of 5 km/s, the Martian meteoroids would spend only a few seconds in the Martian atmosphere; most of the diffusion would occur outside of the Martian atmosphere. To estimate how the Martian surface T would affect our thermal modeling, we calculated fractional He loss during the meteoroid's passage in the lower layer of the Mars atmosphere (<~20 km from the ground) at different ambient temperatures (140–290 K). The resulting He loss is almost identical for the given surface T variations (~150 °C). In contrast, the changes of crystallographic structures or microscopic textures in shocked meteorite occur much more rapidly, within a few seconds, if not a few milliseconds; therefore, texture-based $T_{post\text{-}shock}$ estimation is more sensitive to the ambient T conditions of the Martian crust.

Fig. 7 displays $T_{equi\text{-}shock}$ estimated for Martian meteorites Los Angeles (Min et al., 2004), ALH84001 (Min and Reiners, 2007), Zagami (this study), and ALHA77005 (this study) from the (U-Th)/He thermal modeling, compared with $T_{post\text{-}shock}$ (Nyquist et al., 2001; Fritz et al., 2005) estimated from the traditional methods. The He diffusion-based $T_{equi\text{-}shock}$ shows a general positive correlation with the texture-based $T_{post\text{-}shock}$ estimates (Fig. 7), confirming the previous suggestion that the He deficit in Martian meteorites is primarily controlled by the ejection-related shock event (Schwenzer et al., 2008). For a more quantitative evaluation of the two independent approaches, the $T_{post\text{-}shock}$ must be converted to $T_{equi\text{-}shock}$. The shaded area represents $T_{equi\text{-}shock} = T_{post\text{-}shock} + T_{ambient}$ with the $T_{ambient} = -70 \pm 75$ °C (total $T_{ambient}$ fluctuation of 150 °C assumed as discussed previously). For the most intensively shocked meteorite of ALHA77005, the two independent methods yield consistent results within their uncertainties. However, as the intensity of shock decreases, $T_{equi\text{-}shock}$ estimated from He diffusion modeling becomes higher than expected from $T_{post\text{-}shock}$. Although the cause of such discrepancies is unclear, it is noteworthy that the previous $T_{post\text{-}shock}$ estimates are highly variable for the same samples, particularly for less intensively shocked meteorites, which does not allow for a more quantitative comparison with the $T_{equi\text{-}shock}$ estimates. For example, among the two major data sets, Nyquist et al.'s (2001) $T_{post\text{-}shock}$ estimates are more consistent with $T_{equi\text{-}shock}$ than the Fritz et al. (2005) for the less intensively shocked Zagami and ALH84001. However, for the other two intensively shocked meteorites of ALHA77005 and Los Angeles, Fritz et al.'s (2005) estimates work better with the He diffusion modeling. In summary, the He diffusion-based $T_{equi\text{-}shock}$ estimates are significantly higher than calculated from the $T_{post\text{-}shock}$ for less-intensively shocked meteorites, and the discrepancy between the two independent approaches decreases as the shock intensity increases. While the reason for the discrepancy remains unclear, we prefer the He diffusion-based approach
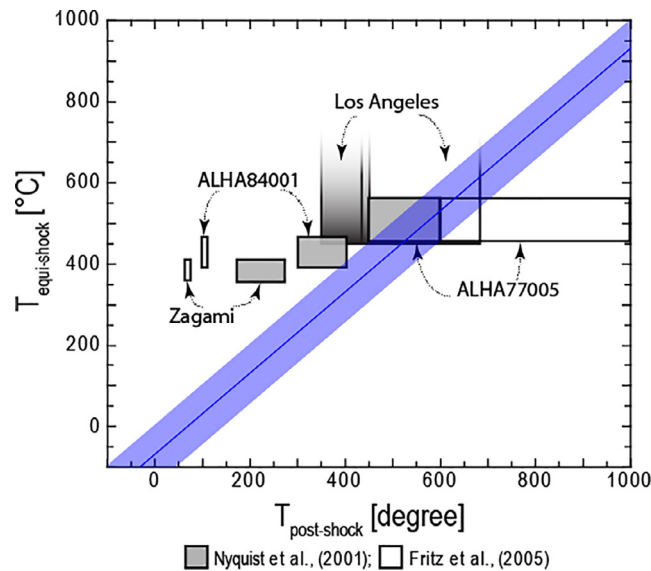
Fig. 7. Comparison between $T_{equi-shock}$ and $T_{post-shock}$ for four Martian meteorites. $T_{equi-shock}$ estimates are from He diffusion modeling in phosphate aggregates. $T_{post-shock}$ estimates are based on refractive indices of feldspars and other textural evidence calibrated against artificially shocked rock samples. The diagonal shaded area represents $T_{equi-shock} = T_{post-shock} + T_{ambient}$ with the $T_{ambient} = -70 \pm 75$ °C. In an ideal case, the $T_{equi-shock}$ and $T_{post-shock}$ data should plot on this area. For intensively shocked meteorites of ALHA77005 and Los Angeles, estimated $T_{equi-shock}$ and $T_{post-shock}$ are generally consistent within their uncertainties. However, as the intensity of shock decreases (ALHA84001 and Zagami), $T_{equi-shock}$ estimated from He diffusion modeling becomes higher than expected from $T_{post-shock}$.

because the $T_{equi-shock}$ estimates are relatively robust to input parameters. The He diffusion-based approach is even more robust for such samples experiencing less intensive shocks, although such samples show a significant discrepancy between the two methods.

One possible way to explain the discrepancy between the two approaches may come from the localized P-T excursion (P-T deviation from equilibrium shock P-T) when a shock wave passed through the meteorite immediately after the shock. To evaluate how such P-T excursion would affect He budget in the sample (and our $T_{equi-shock}$ estimates from the He data), it is necessary to understand (1) the degree of P-T excursion and (2) its time scale. For Zagami, Beck et al. (2005) suggested a localized T increase up to ~2400–2500 K for K-hollandite in a time scale of ~10–30 ms, based on the trace element distributions (Ba, Cs, Sr) near the margin of K-hollandite aggregate. However, the P-T excursion is an extremely localized phenomenon, and it is also very dependent on mineral phases. According to the preliminary work of Fritz and Greshake (2009), the degree and direction of T excursion vary in the co-existing minerals. For a hypothetical meteorite presumably having similar compositions to Martian meteorites, a positive T excursion (~2000 K, above the equilibrium shock T of ~550 K) is expected for plagioclase, and negative T excursions (~400–500 K, below the equilibrium shock T of ~550 K) for pyroxene and olivine, before these minerals reach the equilibrium shock T (~550 K) within a second. However, the direction and degree of T excursion for phosphate, the phase we used for (U-Th)/He dating, are not documented in their study (Fritz and Greshake, 2009). Further model calculations for P-T excursion in phosphate as well as textural evidence supporting this will improve understanding of He budget in the system.

5. CONCLUSIONS

1. (U-Th)/He ages obtained from multiple phosphate aggregates yielded overall ages of 92.2 ± 4.4 Ma (2σ) and 8.4 ± 1.2 Ma for Zagami and ALHA77005, respectively. These estimates are generally consistent with the previously reported whole rock (U-Th)/He ages, but have smaller uncertainties. These ages correspond to fractional losses of 0.49 ± 0.03 and 0.97 ± 0.01 for Zagami and ALHA77005, respectively, assuming that the ejection-related shock event at ~3 Ma is solely responsible for helium loss since crystallization.

2. Detailed examination of fracture patterns in phosphates using SEM yielded FFAs' (Fracture Free Areas') radii of ~2–9 μm and 4–20 μm for Zagami and ALHA77005, respectively. For Zagami, the previously reported isothermal heating experiments for a whole rock sample (Bogard et al., 1984) suggest the diffusion domain radius of 1–4 μm. The consistent results from textural observations using SEM and isothermal heating experiments for Zagami provide compelling evidence for constraints of diffusion domain dimensions.

3. Conductive cooling model combined with the new (U-Th)/He data, diffusion domain radii, and other input parameters yielded $T_{equi-shock}$ estimates of 360–410 °C and 460–560 °C for Zagami and ALHA77005, respectively. These estimates are relatively robust to input parameters. The $T_{equi-shock}$ estimates for Zagami are more robust than those for ALHA77005 primarily because Zagami yielded an intermediate f_{He} value (0.49) compared to ALHA77005 (0.97). Therefore,

Table A1
List of 80 out of 165 Zagami aggregates used for this study.

Batch	Individual aggregate					
	75–125 µm		125–150 µm		150–250 µm	
Z01-20	06 grn01	26 grn01				
	14 grn01	27 grn01				
	15 grn01	30 grn01				
	16 grn01	31 grn01				
	18 grn01	33 grn01				
	18 grn02	33 grn02				
	22 grn01	33 grn03				
	22 grn02	36 grn01				
	22 grn03	38 grn01				
	23 grn01	41 grn01				
Z21-40	42 grn01	52 grn02				
	43 grn01	54 grn01				
	45 grn01	55 grn01				
	45 grn02	58 grn01				
	46 grn01	58 grn02				
	47 grn01	60 grn01				
	47 grn02	64 grn01				
	48 grn01	65 grn01				
	51 grn01	65 grn02				
	52 grn01	65 grn03				
Z41-60	67 grn01		20 grn01	44 grn01		
	68 grn01		25 grn01	51 grn01		
	68 grn02		25 grn02	51 grn02		
	69 grn01		28 grn01	51 grn03		
	71 grn01		29 grn01	64 grn01		
	72 grn01		39 grn01	64 grn02		
	72 grn02		39 grn02			
Z61-80			63 grn01	75 grn01	4 grn01	
			63 grn02	75 grn02	4 grn02	
			63 grn03	86 grn01	5 grn01	
			66 grn01	86 grn02	8 grn01	
			66 grn02	106 grn01		
			68 grn01	112 grn01		
			68 grn02	116 grn01		
			72 grn01	117 grn01		

Zagami's $T_{equi\text{-}shock}$ estimates are less sensitive to major input parameters, such as diffusion domain radius or alpha recoil correction factor.

4. For less intensively shocked Zagami, the He diffusion-based $T_{equi\text{-}shock}$ estimations from this study were significantly higher than expected from the previously reported $T_{post\text{-}shock}$ values. For intensively shocked ALHA77005, these two independent approaches yielded generally consistent results. Including two other Martian meteorites of ALH84001 and Los Angeles, it is suggested that, for intensively shocked meteorites, the He diffusion-based approach yields slightly higher or consistent $T_{equi\text{-}shock}$ with estimation from $T_{post\text{-}shock}$, and the discrepancy between the two methods decreases as the intensity of shock increases. It is also suggested that the He diffusion-based approach provides more robust estimation for $T_{equi\text{-}shock}$ estimation.

APPENDIX A

See Tables A1, A2, A3, and A4.

Table A2
List of 85 out of 165 Zagami aggregates used in this study.

Batch	Individual Aggregate 150–250 μm		Packet	Individual Aggregate 125–150 μm
Z81-92	14 grn01	20 grn01	ZAG01	Zag0011-001
	15 grn01	21 grn01		Zag0022-001
	16 grn01	21 grn02		Zag0023-002
	17 grn01	21 grn03		Zag0026-001
	17 grn02	22 grn01		Zag0038-002
	18 grn01	23 grn01		
			ZAG234	Zag0040-001
Z93-102	24 grn01	31 grn01		Zag0041-001
	27 grn01	31 grn02		Zag0042-001
	28 grn01	31 grn03		Zag0046-001
	30 grn01	31 grn04		Zag0047-001
	30 grn02	32 grn01		Zag0047-002
				Zag0047-003
Z103-113	37 grn01	42 grn02		Zag0047-004
	37 grn02	43 grn01		Zag0049-001
	39 grn01	43 grn02		Zag0052-001
	41 grn01	45 grn01		Zag0059-001
	41 grn02	45 grn02		Zag0059-002
	42 grn01			Zag0059-003
				Zag0060-002
Z114-123	46 grn01	52 grn01		Zag0060-001
	47 grn01	52 grn02		
	48 grn01	52 grn03	ZAG05	Zag0004-001
	48 grn02	54 grn01		Zag0011-002
	50 grn01	54 grn02		Zag0022-001
				Zag0022-002
Z124-134	56 grn01			Zag0065-001
	56 grn02			Zag0069-001
	57 grn01			Zag0070-001
	58 grn01			Zag0083-001
	58 grn02			Zag0083-002
	58 grn03			Zag0093-001
	59 grn01			Zag0100-001
	59 grn02			
	61 grn01			
	61 grn02			
	61 grn03			

Table A3
List of 56 out of 83 ALHA77005 aggregates used in this study.

Batch	Individual aggregate 63–150 μm		>180 μm
A01-20	02 grn01	15 grn02	
	03 grn01	15 grn03	
	03 grn02	16 grn01	
	04 grn01	16 grn02	
	04 grn02	17 grn01	
	08 grn01	17 grn02	
	08 grn02	18 grn01	
	09 grn01	19 grn01	
	11 grn01	20 grn01	
	15 grn01	20 grn02	

Table A3 (*continued*)

Batch	Individual aggregate			
	63–150 μm		>180 μm	
A21-40	21 grn01	29 grn03		
	22 grn01	39 grn01		
	22 grn02	39 grn02		
	23 grn01	42 grn01		
	27 grn01	45 grn01		
	27 grn02	46 grn01		
	28 grn01	46 grn02		
	28 grn02	47 grn01		
	29 grn01	51 grn01		
	29 grn02	51 grn02		
A41-56	49 grn01	64 grn01	32 grn01	51 grn01
	53 grn01	66 grn01	36 grn01	55 grn01
	59 grn01	66 grn02	37 grn01	55 grn02
	60 grn01	66 grn03	44 grn01	56 grn01

Table A4
List of 27 out of 83 ALHA77005 aggregates used in this study.

Batch	Individual aggregate		
	63–150 μm	150–180 μm	
AHp123	Cu0010130-01	Cu0020039-01	Cu0030008-01
	Cu0010046-02	Cu0020006-01	Cu0030012-01
	Cu0010042-01	Cu0030005-01	Cu0030020-01
	Cu0010027-03	Cu0030006-01	Cu0030022-01
	Cu0010030-02	Cu0030007-01	Cu0030023-01
AHp45		Cu0030030-01	Cu0030048-01
		Cu0030032-01	Cu0030052-01
		Cu0030039-01	Cu0030060-01
		Cu0030040-01	Cu0030062-01
		Cu0030045-01	Cu0030067-02
		Cu0030046-01	Cu0030075-01

REFERENCES

Aciego S., Kennedy B. M., DePaolo D. J., Christensen J. N. and Hutcheon I. (2003) U-Th/He age of phenocrystic garnet from the 79 AD eruption of Mt. Vesuvius. *Earth Planet. Sci. Lett.* **216**, 209–219.

Ahrens T. J. and Gregson V. G. J. (1964) Shock compression of crustal rocks: data for quartz, calcite, and plagioclase rocks. *J. Geophys. Res.* **69**, 4839–4874.

Ahrens T. J., Petersen C. F. and Rosenberg J. T. (1969) Shock compression of feldspars. *J. Geophys. Res.* **74**, 2727–2746.

Alexeev V. A. (1998) Parent bodies of L and H chondrites: times of catastrophic events. *Meteorit. Planet. Sci.* **33**, 145–152.

Arrol W. J., Jacobi R. B. and Paneth F. A. (1942) Meteorites and the age of the solar system. *Nature* **149**, 235–238.

Artemieva N. and Ivanov B. A. (2004) Launch of Martian meteorites in oblique impacts. *Icarus* **171**, 84–101.

Ash R. D., Knott S. F. and Turner G. (1996) A 4-Gyr shock age for a Martian meteorite and implications for the cratering history of Mars. *Nature* **380**, 57–59.

Bauer C. A. (1947) Production of helium in meteorites by cosmic radiation. *Phys. Rev.* **72**, 354–355.

Beck P., Gillet P., El Goresy A. and Mostefaoui S. (2005) Timescales of shock processes in chondritic and Martian meteorites. *Nature* **435**, 1071–1074.

Becker R. H. and Pepin R. O. (1984) The case for a Martian origin of the shergottites: nitrogen and noble gases in EETA79001. *Earth Planet. Sci. Lett.* **69**, 225–242.

Bogard D. D. and Garrison D. H. (1999) Argon-39-argon-40 "ages" and trapped argon in Martian shergottites, Chassigny, and ALH84001. *Meteorit. Planet. Sci.* **34**, 451–473.

Bogard D. D. and Hirsch W. C. (1980) 40Ar/39Ar dating, Ar diffusion properties, and cooling rate determinations of severely shocked chondrites. *Geochim. Cosmochim. Acta* **44**, 1667–1682.

Bogard D. D. and Johnson P. (1983) Martian ages in an Antarctic meteorite. *Science* **221**, 651–654.

Bogard D. D. and Park J. (2008) [39]Ar-[40]Ar dating of the Zagami Martian shergottite and implications from magma origin of excess [40]Ar. *Meteorit. Planet. Sci.* **43**, 1113–1126.

Bogard D. D., Husain L. and Nyquist L. E. (1979) 40Ar-39Ar age of the Shergotty achondrite and implications for its post-shock thermal history. *Geochim. Cosmochim. Acta* **43**, 1047–1056.

Bogard D. D., Nyquist L. E. and Johnson P. J. (1984) Noble gas contents of shergottites and implications for the Martian origin of SNC meteorites. *Geochim. Cosmochim. Acta* **48**, 1723–1739.

Bogard D. D., Horz F. and Johnson P. H. (1986) Shock-implanted noble gases: an experimental study with implications for the origin of Martian gases in shergottite meteorites. *J. Geophys. Res.* **91**, E99–E114.

Bouvier A., Blichert-Toft J., Vervoort J. D., Gillet P. and Albarede F. (2008) The case for old basaltic shergottites. *Earth Planet. Sci. Lett.* **266**, 105–124.

Bouvier A., Blichert-Toft J. and Albarede F. (2009) Martian meteorite chronology and the evolution of the interior of Mars. *Earth Planet. Sci. Lett.* **280**, 285–295.

Bouvier A., Blichert-Toft J. and Albarede F. (2014) Comment on "Geochronology of the Martian meteorite Zagami revealed by U-Pb ion probe dating of accessory minerals by Zhou et al. *Earth Planet. Sci. Lett.* **385**, 216–217.

Butler C. P. (1966) Temperatures of meteoroids in space. *Meteoritics* **3**, 59–70.

Cassata W. S., Shuster D. L., Renne P. R. and Weiss B. P. (2010) Evidence for shock heating and constraints on Martian surface temperatures revealed by $^{40}Ar/^{39}Ar$ thermochronometry of Martian meteorites. *Geochim. Cosmochim. Acta* **74**, 6900–6920.

El Goresy A., Gillet P., Miyahara M., Ohtani E., Ozawa S., Beck P. and Montagnac G. (2013) Shock-induced deformation of Shergottites: shock-pressure and perturbations of magmatic ages on Mars. *Geochim. Cosmochim. Acta* **101**, 233–262.

Eugster O. (1988) Cosmic-ray production rates for ^{3}He, ^{21}Ne, ^{38}Ar, ^{83}Kr, and ^{126}Xe in chondrites based on ^{81}Kr-Kr exposure ages. *Geochim. Cosmochim. Acta* **52**, 1649–1662.

Eugster O., Weigel A. and Polnau E. (1997) Ejection times of Martian meteorites. *Geochim. Cosmochim. Acta* **61**, 2749–2757.

Eugster O., Busemann H., Lorenzetti S. and Terribilini D. (2002) Ejection ages from krypton-81-krypton-83 dating and pre-atmospheric sizes of Martian meteorites. *Meteorit. Planet. Sci.* **37**, 1345–1360.

Farley K. A. (2000) Helium diffusion from apatite: general behavior as illustrated by Durango fluorapatite. *J. Geophys. Res.* **105**, 2903–2914.

Fritz J. and Greshake A. (2009) Petrographic constraints on shock induced P/T conditions in shergottites (Abstract). *Lunad and Planetary Science Conference* **40**, 1581.

Fritz J., Artemieva N. and Greshake A. (2005) Ejection of Martian meteorites. *Meteorit. Planet. Sci.* **40**, 1393–1411.

Heymann D. (1967) On the origin of hypersthene chondrites: ages and shock effects of black chondrites. *Icarus* **6**, 189–221.

Hofmeister A. M. (1999) Mantle values of thermal conductivity and geotherm from Photon lifetime. *Science* **283**, 1699–1706.

Leya I. and Masarik J. (2009) Cosmogenic nuclides in stony meteorites revisited. *Meteorit. Planet. Sci.* **44**, 1061–1086.

Lodders K. (1998) A survey of SNC meteorite whole-rock compositions. *Meteorit. Planet. Sci.* **33**, A183–A190.

Lu R., Hofmeister A. M. and Wang Y. (1994) Thermodynamic properties of ferromagnesium silicate perovskites from vibrational spectroscopy. *J. Geophys. Res.* **99**, 11795–11804.

McSween, Jr., H. Y. (2002) The rocks of Mars, from far and near. *Meteorit. Planet. Sci.* **37**, 7–25.

Melcher C. L. (1979) Kirin meteorite: temperature gradient produced during atmospheric passage. *Meteoritics* **14**, 309–316.

Melosh H. J. (1984) Impact ejection, spallation, and the origin of meteorites. *Icarus* **59**, 234–260.

Melosh H. J. (1989) *Impact Cratering: A Geologic Process*. Oxford University Press, New York, p. 253.

Min K. (2005) Low-temperature thermochronometry of meteorites. In *Reviews in Mineralogy and Geochemistry* (eds. P. W. Reiners and T. A. Ehlers). Mineralogical Society of America Geochemical Society, pp. 567–588.

Min K. and Reiners P. W. (2007) High-temperature Mars-to-Earth transfer of meteorite ALH84001. *Earth Planet. Sci. Lett.* **260**, 72–85.

Min K., Farley K. A., Renne P. R. and Marti K. (2003) Single grain (U-Th)/He ages from phosphates in Acapulco meteorite

and implications for thermal history. *Earth Planet. Sci. Lett.* **209**, 323–336.

Min K., Reiners P. W., Nicolescu S. and Greenwood J. P. (2004) Age and temperature of shock metamorphism of Martian meteorite Los Angeles from (U-Th)/He thermochronometry. *Geology* **32**, 677–680.

Min K., Reiners P. W. and Shuster D. L. (2013) (U–Th)/He ages of phosphates from St. Séverin LL6 chondrite. *Geochim. Cosmochim. Acta* **100**, 282–296.

Mitchell S. G. and Reiners P. W. (2003) Influence of wildfires on apatite and zircon (U-Th)/He ages. *Geology* **31**, 1025–1028.

Nishiizumi K., Kleine J., Middleton R., Elmore D., Kubic P. W. and Arnold J. R. (1986) Exposure history of shergottites. *Geochim. Cosmochim. Acta* **50**, 1017–1021.

Nyquist L. E., Bogard D. D., Shih C.-Y., Greshake A., Stöffler D. and Eugster O. (2001) Ages and geologic histories of Martian meteorites. *Space Sci. Rev.* **96**, 105–164.

Opeil C. P., Consolmagno G. J. and Britt D. T. (2010) The thermal conductivity of meteorites: new measurements and analysis. *Icarus* **208**, 449–454.

Opeil S. J. C. P., Consolmagno S. J. G. J., Safarik D. J. and Britt D. T. (2012) Stony meteorite thermal properties and their relationship with meteorite chemical and physical properties. *Meteorit. Planet. Sci.* **47**, 319–329.

Owen T., Biemann K., Rushneck D. R., Biller J. E., Howarth D. W. and Lafleur A. L. (1977) The composition of the atmosphere at the surface of Mars. *J. Geophys. Res.* **82**, 4635–4639.

Paneth F. A., Urry W. D. and Koeck W. (1930) The age of iron meteorites. *Nature* **125**, 490–491.

Paneth F. A., Reasbeck P. and Mayne K. I. (1952) Helium 3 content and age of meteorites. *Geochim. Cosmochim. Acta* **2**, 300–303.

Park J., Bogard D. D., Nyquist L. E. and Herzog G. F. (2014) Issues in dating young rocks from another planet: Martian shergottites. *Geol. Soc. London, Spec. Publ.* **378**, 297–316.

Reiners P. W. and Farley K. A. (1999) He diffusion and (U-Th)/He thermochronometry of titanite. *Geochim. Cosmochim. Acta* **63**, 3845–3859.

Reiners P. W. and Farley K. A. (2001) Influence of crystal size on apatite (U-Th)/He thermochronology: an example from the Bighorn Mountains, Wyoming. *Earth Planet. Sci. Lett.* **188**, 413–420.

Reiners P. W., Farley K. A. and Hickes H. J. (2002) He diffusion and (U-Th)/He thermochronometry of zircon: initial results from Fish Canyon Tuff and Gold Butte, Nevada. *Tectonophysics* **349**, 297–308.

Reiners P. W., Thomson S. N., McPhillips D., Donelick R. A. and Roering J. J. (2007) Wildfire thermochronology and the fate and transport of apatite in hillslope and fluvial environments. *J. Geophys. Res.-Earth Surf.* **112**, F04001. http://dx.doi.org/10.1029/2007JF000759.

Schnabel C., Ma P., Herzog G. F., Faestermann T., Knie K. and Korschinek G. (2001) ^{10}Be, ^{26}Al, and ^{53}Mn in Martian meteorites (Abstract). *Lunar and Planetary Science*, XXXII, p. 1353.

Schultz L. and Franke L. (2004) Helium, neon, and argon in meteorites: a data collection. *Meteorit. Planet. Sci.* **39**, 1889–1890.

Schwenzer S. P., Fritz J., Greshake A., Herrmann S., Jochum K. P., Ott U., Stöffler D. and Stoll B. (2004) Helium loss and shock pressure in Martian meteorites – a relationship (Abstract). *Meteorit. Planet. Sci.* **39**, A96.

Schwenzer S. P., Herrmann S., Mohapatra R. K. and Ott U. (2007) Noble gases in mineral separates from three shergottites: Shergotty, Zagami, and EETA79001. *Meteorit. Planet. Sci.* **42**, 387–412.

Schwenzer S. P., Fritz J., Stöffler D., Trieloff M., Amini M., Greshake A., Herrmann S., Herwig K., Jochum K. P., Mohapatra R. K., Stoll B. and Ott U. (2008) Helium loss from Martian meteorites mainly induced by shock metamorphism: evidence from new data and a literature compilation. *Meteorit. Planet. Sci.* **43**, 1841–1859.

Shan J., Min K. and Nouiri A. (2013) Thermal effects of scanning electron microscopy on He diffusion in apatite: Implications for (U-Th)/He dating. *Chem. Geol.* **345**, 113–118.

Shuster D. L. and Weiss B. P. (2005) Martian surface paleotemperatures from thermochronology of meteorites. *Science* **309**, 594–597.

Stöffler D. (1971) Progressive metamorphism and classification of shocked and brecciated crystalline rocks at impact craters. *J. Geophys. Res.* **76**, 5541–5551.

Stöffler D. and Langenhorst F. (1994) Shock metamorphism of quartz in nature and experiment: I. Basic observation and theory. *Meteoritics* **29**, 155–181.

Stöffler D., Ostertag R., Jammes C., Pfannschmidt G., Sen Gupta P. R., Simon S. M., Papike J. J. and Beauchamp R. H. (1986) Shock metamorphism and petrography of the Shergotty achondrite. *Geochim. Cosmochim. Acta* **50**, 889–903.

Stöffler D., Bischoff A., Buchwald U. and Rubin A. E. (1988) Shock effects in meteorites. In *Meteoritics and the Early Solar System* (eds. J. F. Kerridge and M. S. Mathews). University of Arizona Press, Tucson, pp. 165–205.

Stöffler D., Keil K. and Scott E. R. D. (1991) Shock metamorphism or ordinary chondrites. *Geochim. Cosmochim. Acta* **55**, 3845–3867.

Strutt R. J. (1908) On the accumulation of helium in geological time. *Proc. R. Soc. London, A* **81**, 272–277.

Strutt R. J. (1909) The accumulation of helium in geological time. II. *Proc. R. Soc. London, A* **83**, 96–99.

Strutt R. J. (1910) The accumulation of helium in geological time. III. *Proc. R. Soc. London, A* **83**, 298–301.

Swindle T. D., Grier J. A. and Burkland M. K. (1995) Noble gases in orthopyroxenite ALH84001: a different kind of Martian meteorite with an atmospheric signature. *Geochim. Cosmochim. Acta* **59**, 793–801.

Tellmann S., Patzold M., Hausler B., Hinson D. P. and Leonard Tyler G. (2013) The structure of Mars lower atmosphere from Mars Express Radio Science (MaRS) occultation measurements. *J. Geophys. Res.* **118**, 306–320.

Turner G., Knott S. F., Ash R. D. and Gilmour J. D. (1997) Ar-Ar chronology of the Martian meteorite ALH84001: evidence for the timing of the early bombardment of Mars. *Geochim. Cosmochim. Acta* **61**, 3835–3850.

Ulrich R., Kral T., Chevrier V., Pilgrim R. and Roe L. (2010) Dynamic temperature fields under Mars landing sites and implications for supporting microbial life. *Astrobiology* **10**, 643–650.

Walton E. L., Kelley S. P. and Spray J. G. (2007) Shock implantation of Martian atmospheric argon in four basaltic shergottites: a laser probe $^{40}Ar/^{39}Ar$ investigation. *Geochim. Cosmochim. Acta* **71**, 497–520.

Waples D. W. and Waples J. S. (2004) A review and evaluation of specific heat capacities of rocks, minerals and subsurface fluids. Part I: minerals and non-porous rocks. *Nat. Resour. Res.* **13**, 97–122.

Wasson J. T. and Wang S. (1991) The histories of ordinary chondrite parent bodies: U, Th-He age distributions. *Meteoritics* **26**, 161–167.

Weiss B. P., Shuster D. L. and Stewart S. T. (2002) Temperature on Mars from $^{40}Ar/^{39}Ar$ thermochronology of ALH84001. *Earth Planet. Sci. Lett.* **201**, 465–472.

Wetherill G. W. (1975) Late heavy bombardment of the moon and terrestrial planets. *Proceedings of the 6th Lunar Science Conference*, 1539-1561.

Wieler R. (2002) Cosmic-ray-produced noble gases in meteorites. In *Reviews in Mineralogy amd Geochemistry* (eds. D. Porcelli, C. J. Ballentine and R. Wieler). Geochemical Society, Mineralogical Society of America, pp. 125–170.

Yin Q.-Z., Herd C. D. K., Zhou Q., Li X.-H., Wu F.-Y., Li Q.-L., Liu Y., Tang G.-Q. and McCoy T. J. (2014) Reply to comment on "Geochronology of the Martian meteorite Zagami revealed by U-Pb ion probe dating of accessory minerals". *Earth Planet. Sci. Lett.* **385**, 218–220.

Zhou Q., Herd C. D. K., Yin Q.-Z., Li X.-H., Wu F.-Y., Li Q.-L., Liu Y., Tang G.-Q. and McCoy T. J. (2013) Geochronology of the Martian meteorite Zagami revealed by U-Pb ion probe dating of accessory minerals. *Earth Planet. Sci. Lett.* **374**, 156–163.

Associate editor: David Shuster